



# Reactive DC Magnetron Sputtered NbN Films on Mild Steel with Electroless Nickel Interlayer

**Kulwant Singh<sup>1\*</sup>, M. R. Gonal<sup>1</sup> and N. Krishnamurthy<sup>1</sup>**

<sup>1</sup>*Materials Group, Bhabha Atomic Research Centre, Trombay, Mumbai-400085, India.*

## **Authors' contributions**

*This work was carried out in collaboration between all authors. Author KS designed the study, carried out the study, wrote the protocol and wrote the first draft of the manuscript. Author MRG performed the XRD analysis and author NK guided the experimental plan, corrected the manuscript and analyzed the results. All authors read and approved the final manuscript.*

**Original Research Article**

**Received 4<sup>th</sup> October 2013  
Accepted 9<sup>th</sup> March 2014  
Published 22<sup>nd</sup> March 2014**

## **ABSTRACT**

**Aims:** To explore the benefits of NbN coating on mild steel (MS) with electroless nickel (EN) interlayer.

**Study Design:** To deposit NbN coatings at various N<sub>2</sub>/Ar flow-ratios and substrate biasing; optimize the parameters and then deposit NbN on MS with EN interlayer.

**Place and Duration of Study:** Material Processing Division, Bhabha Atomic Research Centre, Trombay, Mumbai, between June 2010 and July 2012.

**Methodology:** NbN was deposited by reactive DC magnetron sputtering varying N<sub>2</sub>/Ar flow ratio between 5-70% and substrate biasing from zero to -150V. Coatings were studied for thickness, hardness, phase analysis and adhesion. Effect of EN interlayer was studied for improvement in hardness, adhesion and corrosion. Corrosion was studied using potentiodynamic polarization technique in 1N H<sub>2</sub>SO<sub>4</sub> solution at room temperature.

**Results:** X-ray diffraction showed hexagonal  $\beta$ Nb<sub>2</sub>N, cubic  $\delta$ NbN and hexagonal  $\delta'$ NbN phases with increasing N<sub>2</sub>. EN layer was found to be amorphous. When NbN top-coat was deposited by sputtering, EN structure changed to crystalline Ni<sub>3</sub>P and Ni. Surface hardness increased from 1084HK<sub>25</sub> for NbN/MS to 1436, 1564 and 1612HK<sub>25</sub> with EN interlayer in 2, 4 and 10 $\mu$ m thickness respectively. In the scratch tests, critical load for cohesive failure varied between 6-8N, 8-15N and 8-18N and critical load for adhesive failure varied between 9-12N, 12-25N and 10-28N for NbN coating on MS, SS and MS/EN

\*Corresponding author: E-mail: singhkw@barc.gov.in;

respectively. Coefficient of friction ( $\mu$ ) in the scratch adhesion tests for NbN/MS was 0.28 at 30N, 0.35 at 40N and 0.45 at 60N load; for NbN/EN/MS,  $\mu$  decreased to 0.22, 0.28 and 0.37 at 30, 40 and 60N loads respectively, demonstrating the improvement. Corrosion studies showed that  $I_{corr}$  decreased from  $150.2\mu A/cm^2$  for NbN/MS to 2.3, 0.37 and  $0.35\mu A/cm^2$  with 2, 4 and  $10\mu m$  thick EN interlayer respectively.

**Conclusion:** There was considerable improvement in the hardness, corrosion resistance and adhesion of NbN/MS, when incorporated with EN interlayer.

**Keywords:** Magnetron-sputtering; NbN; electroless nickel; corrosion; adhesion; hardness.

## 1. INTRODUCTION

Hard nitride coatings deposited by physical vapor deposition (PVD) techniques exhibit high hardness, good wear resistance and excellent chemical inertness. Magnetron Sputtering is widely used for deposition of hard nitride coatings [1-4]. Studies have been carried out to explore the sputtered nitride coating on mild steel (MS) substrate with various interlayers [5-9]. Extending the hard nitride coatings on MS requires interlayer because—

1. Nitride coatings being too hard ( $>1800\text{ Kg/mm}^2$ ), require good load support.
2. Though PVD coatings are highly inert, they have inherent pin-hole porosity. Therefore, these coatings may not protect the MS effectively. Intermediate layer provides barrier to the corrosive environment, besides improving adhesion.

Good mechanical properties coupled with chemical inertness, wear resistance, high melting point, and temperature stability make niobium nitride (NbN) films a suitable material for protective coating [10] and diffusion barrier in microelectronic devices [11]. The deposition of NbN films have been carried out by reactive magnetron sputtering [12-15], ion beam assisted deposition [16,17], pulsed laser deposition [18] and cathodic arc deposition [19-22].

TiN coatings with chromium, nickel or electroless nickel (EN) interlayer have been found to improve hardness, corrosion resistance and other properties when extended on to MS substrate [5-9]. In the present study, NbN coatings have been explored on MS with EN interlayer. NbN was deposited by reactive DC magnetron sputtering. EN was deposited by electroless deposition technique. NbN coatings were first deposited on stainless steel (SS) substrates, process parameters were optimized and then NbN coatings as such and with EN interlayer were deposited on MS substrates. Duplex coatings have been studied for the improvement in hardness, adhesion and corrosion resistance. Adhesion was evaluated by scratch test, surface hardness was measured by Knoop micro indentation and corrosion was performed by potentiodynamic polarization technique. Open circuit potentials (OCP) were also measured.

## 2. MATERIALS AND METHODS

The NbN films were deposited using reactive DC magnetron sputtering on SS, MS and EN plated MS substrates. A niobium (99.97% purity) metallic target, 160mm diameter and 4mm thick, was mechanically clamped to a planar sputter source. Chamber was evacuated to a base pressure of  $2\times 10^{-6}\text{mbar}$ . Distance between the target and the substrate was set at 60mm. The sputtering pressure was kept at  $5\times 10^{-3}\text{mbar}$  by admitting a stream of mixed gas of argon (Ar) and nitrogen (N<sub>2</sub>) into the chamber. Flow of Ar gas was fixed at 20scm while

$N_2$  flow was varied from 1-14sccm. Substrate was biased at -50V for the coatings deposited at different  $N_2$  flows. The power to the target was supplied through a stabilized d. c. power supply of 0-1000V (6 Amperes maximum). Substrate biasing was varied from zero (unbiased externally) to -150V in a step of 25V (keeping the  $N_2$ /Ar flow ratio constant at 20%). Power supply used for biasing was a stabilized d. c. power supply of variable voltage (0-300V) and current (0-500mA). The samples were polished, cleaned sequentially in alkali solution, methyl alcohol and acetone prior to the deposition. All the cleaning steps were performed ultrasonically. For electroless plating, the MS samples were etched in 30% hydrochloric acid after rinsing with distill water. It was necessary to ensure complete surface wetting, such that water film covers the sample surface before plating. Composition of the bath used and operating parameters for electroless plating of nickel are listed in Table 1. MS samples after conventional pre-treatment, were plated with EN by varying the duration of plating. The rate of deposition was first determined on a separate sample plated under similar conditions. Duration of plating was varied to obtain the thicknesses of 2, 4 and 10  $\mu m$ .

**Table 1. Composition of bath and operating parameters for EN plating**

Parameters	Value	Parameters	Value
Nickel chloride	35 g/l	Stabilizer	1-2 ppm
Sodium citrate	20 g/l	Agitation of bath	Continuous
Sodium hypophosphite	20 g/l	Temperature	$\sim 90^0C$
pH	4.4 - 4.6		

Thickness of the coatings was calculated by weight gain method using bulk density value. Actual coating thickness was found out by using Calo test technique, where coated samples were abraded by an AISI 52100 hardened chrome steel ball (hardness = 65HRC) using suspended diamond particles. The phase structure of the films was investigated by X-ray diffraction (XRD) (make DIANO) at 20mA and 35kV using  $CuK_{\alpha}$  radiation. Surface hardness was measured by a microhardness tester (Future Tech FM-7 model) using Knoop indenter at loads of 100, 50 and 25gf. Five readings were performed for each sample and at each load and the average values are reported. NbN coatings on MS and SS were evaluated for their adhesion performance by scratch adhesion tester (CSM Revetester) at different loading rates of 10, 30, 50 and 80N/min. The scratch indenter used was a 200 $\mu m$  tip radius Rockwell type diamond indenter and the scratch length was 4mm. Friction force and coefficient of friction for all the scratched samples were recorded online during the scratch. The scratch tracks were seen in the optical microscope immediately after the tests to observe the scratch patterns and pictures were taken at different loads. Tests were performed in a linearly progressive mode with a starting load of 1N while maximum load was varied from 10N to 60N.

Potentiodynamic measurement technique was employed to evaluate the electrochemical behavior of coated samples using a computer controlled Santronic Electrochemical Analyzer. Tests were carried out using a three-electrode cell. Samples coated on one side were soldered (with indium) to a copper wire on the other side. The samples were masked by Shailmask 800 lacquer (proprietary) to get the 1cm<sup>2</sup> surface area exposed. All potentials were measured with respect to a saturated calomel electrode (SCE). The auxiliary or counter electrode was platinum. The anodic and cathodic electrochemical polarization curves of all the samples were obtained in nitrogen de-aerated 1N sulphuric acid electrolyte at room temperature. OCP were measured in deaerated 1N sulfuric acid solution for 2hrs. Before potentiodynamic measurements, the samples were allowed to reach equilibrium potential ( $E_{ocp}$ ). This potential was reached after 30-60 minutes and the electrochemical

measurements were started when the potential did not change by more than 1mV/min. The solution was replaced after each sweep run. Polarization resistance was determined in the  $\pm 15\text{mV}$  domain of  $E_{\text{oep}}$  potential using the linear polarization method at a scan rate of  $0.1\text{mV/sec}$ . For potentiodynamic studies a potential sweep range of  $-1.000\text{V}$  to  $+1.000\text{V}$  was applied with a scan rate of  $0.5\text{mV/sec}$ . The plot of  $E$  (measured against SCE) v/s  $\log I$  was plotted. The corrosion potential ( $E_{\text{corr}}$ ) was determined from the intersection of Tafel slopes. Corrosion current density ( $I_{\text{corr}}$ ) was calculated using the anodic and cathodic Tafel slopes ( $\beta_a$  and  $\beta_c$ ) and polarization resistance ( $R_p$ ).

### 3. RESULTS AND DISCUSSION

#### 3.1 Thickness

NbN coating with thickness of about  $1.8\mu\text{m} \pm 10\%$  was obtained. A variation of 5-15% was found in the calculated and actual thickness values. This was because the density of the coatings deposited by PVD techniques is generally lower than the bulk value. The density of CrN coatings deposited by magnetron sputtering has been found to be lower than the nominal density of CrN [23]. In general, increasing substrate bias increased the coating density. In the deposition using biasing there was a continuous ion bombardment at the substrate, causing the reduced effective deposition rate. Therefore more time was required to get the same coating thickness for coatings deposited at higher bias voltages. Thickness of EN plating on MS substrates was 2, 4 and  $10\mu\text{m}$ .

#### 3.2 Phase Analysis

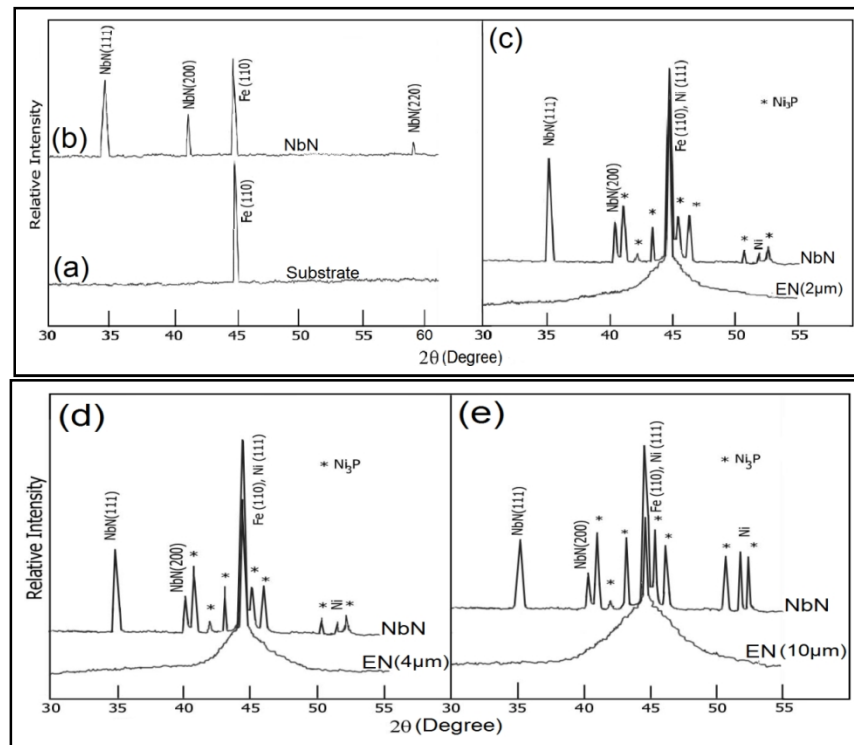
Coatings deposited at 5% of  $F_{\text{N}_2}/F_{\text{Ar}}$  showed hexagonal  $\beta$  Nb<sub>2</sub>N as the major phase with (101) preferred orientation. With increase in  $F_{\text{N}_2}/F_{\text{Ar}}$  to 10% the major phase became cubic  $\delta$  NbN with preferred orientation of (111). At 30%  $F_{\text{N}_2}/F_{\text{Ar}}$  hexagonal  $\delta'$  NbN phase appeared, though the major phase was still cubic  $\delta$  NbN but now with preferred orientation of (200). With further increase in N<sub>2</sub> flow the hexagonal  $\delta'$  NbN phase increased and became a major phase at 70% of  $F_{\text{N}_2}/F_{\text{Ar}}$ . In all the coatings substrate peaks were identified as the major peaks. The XRD patterns obtained for NbN have been shown and discussed in one of our earlier work [24].

Fig.1 shows the XRD pattern of MS substrate, NbN/MS, EN/MS and NbN/EN/MS. MS sample showed the Fe (110) peak in the  $2\theta$  range performed. NbN coating showed the cubic  $\delta$  NbN phase with (111) peak stronger than (200) and (220) peaks. EN structure was amorphous having a diversion at Fe (110) / Ni (111). This peak was found to be shortening and getting broadened with the increase in thickness of EN. The broad and sharp peaks, also observed by Wu et al [25], indicate the amorphous nickel–phosphorous solid solution with Ni crystalline structure of the as-deposited Ni–P film. When NbN top-coat was deposited by sputtering, several peaks of Ni<sub>3</sub>P and Ni were observed. This clearly demonstrates the transformation of EN structure from amorphous to crystalline, during sputtering. This was due to the energy transferred by bombarding ions during sputtering.

#### 3.3 Hardness

Surface hardness for Nb-N/SS (at a load of 25gf) was found to increase with the increase in N<sub>2</sub> flow initially. Hardness reached a maximum value of 2040HK at  $F_{\text{N}_2}/F_{\text{Ar}}=20\%$  and then

decreased with the further increase in N<sub>2</sub> flow [24]. It is known that there are many factors that would affect the hardness of the film, such as defect density, stoichiometry, preferred orientation, residual stress and grain size. Previous studies [26,27] have reported that preferred orientation is a very important factor to the film hardness and <111> is the hardest orientation in the TiN film due to geometrical strengthening. The hardness is expected to increase as the <111> texture coefficient increases. Since NbN has the same NaCl crystal structure as TiN, <111> is supposed to be the hardest orientation of the NbN film. The <111> peak intensity increased till N<sub>2</sub>/Ar flow ratio of 20% and then decreased with the further increase in N<sub>2</sub> flow. The increase in hardness up to 3200 kg/mm<sup>2</sup> for TiN coating with increase in nitrogen content up to 40 at% and thereafter decrease in hardness was observed by Saoula et al [28]. The decrease in hardness in our study after 30% N<sub>2</sub>/Ar flow ratio was accompanied with the observed changes in the crystalline structure of the coatings. Besides, grain size also influences the hardness of the materials. Hardness decreases with the increase in grain size as per the Hall-Petch relationship ( $\sigma_y = \sigma_i + K/\sqrt{D}$ ), where  $\sigma_y$ = yield point, d=grain size for a polycrystalline material, and  $\sigma_i$ = shear stress required to ensure gliding dislocations in a mono crystal, and K is a constant individual for each material also known as the Hall-Petch parameter. Grain size has been found to increase with the increase in partial pressure of N<sub>2</sub> in the previous studies [29-31]. The decrease in hardness at higher N<sub>2</sub> flow could, therefore, be attributed partly to the change in orientation and crystal structure and partly to the increase in grain size. Since, the maximum hardness obtained was at 20% of F<sub>N2</sub>/F<sub>Ar</sub>, NbN deposition on MS (with EN interlayer) was carried out at F<sub>N2</sub>/F<sub>Ar</sub> of 20%.



**Fig. 1. X-ray diffraction patterns for (a) MS substrate; (b) NbN/MS; (c) EN(2μm)/MS and NbN/EN(2μm)/MS; (d) EN(4μm)/MS and NbN/EN(4μm)/MS; (e) EN(10μm)/MS and NbN/EN(10μm)/MS**

Increase in substrate biasing voltage caused the hardness to increase continuously [24]. Hardness increased from 1692HK (for coating deposited without biasing) to 2346HK (for coating deposited at -150V substrate biasing). Kim et al [12] observed the increase in hardness similarly with the increase in substrate bias voltage up to -200V. Increase in hardness was due to the increased ion bombardment with every increase in substrate biasing. The hardness enhancement by energetic ion bombardment is due to a complex, synergistic effect involving a decrease of crystallite size, densification of the grain boundaries, formation of point defects and generation of compressive stress [32]. The development of the morphology and microstructure of sputtered films bombarded by energetic ions during their growth is described by the Thornton diagram [33]. It is well known that ion bombardment due to biasing (the substrate) generally causes a reduction of the grain size [33, 34]. The increased ion flux with higher kinetic energy provides increased ion bombardment on the growing film, which leads to a reduction in the grain size. Hardness increases with the refinement of the grain structure. Hardness is also found to be correlated directly to the compressive stresses. Similar enhancement in the hardness and increased compressive stress has also been reported for a variety of hard coatings deposited by magnetron sputtering [35] and vacuum arc deposition [36].

The surface hardness of MS substrate, EN/MS, NbN/MS, and NbN/EN/MS are given in Table 2. EN plating, was found to show the surface hardness of about 500-600HK. Increase in hardness, in general, is evident with the decrease in load and increase in the thickness of deposits. This was due to the substrate effect. Since the MS substrate has a lower hardness of about 180-200HK, a thin coating on it will not show the true hardness of the coating. The hardness value, in fact, will be a composite hardness of the substrate and the coating. The substrate effect will decrease with the increasing thickness of the coating or with the decrease in the applied load. As a thumb rule, coating thickness should be about 10 times the depth of indentation obtained during hardness test to get the true hardness of the coating. Surface hardness of NbN coating increased from 487 to 1084HK with the decrease in applied load from 100 to 25gf. With the incorporation of EN interlayer, the surface hardness of NbN/MS increased due to the load support provided by the interlayer, since EN has higher hardness than the MS substrate. Hardness increased with the increase in the thickness of interlayer. In a similar study by Wu et al [25] it was found that CrN/MS did not show much hardness, an interesting result was found with the incorporation of EN interlayer; the hardness of the CrN/MS assembly increased to as high as 2500HK. Accordingly, the beneficial effect of the coating assembly modified by the EN interlayer is evident.

**Table 2. Surface hardness for EN, NbN and duplex coatings on MS**

Coating (thickness $\mu\text{m}$ )	100gf	50gf	25gf	Coating (thickness $\mu\text{m}$ )	100gf	50gf	25gf
Substrate	182	186	198	NbN	487	674	1084
EN (2)	326	381	439	EN (2) + NbN	712	905	1436
EN (4)	447	489	586	EN (4) + NbN	892	1078	1564
EN (10)	582	592	612	EN (10) + NbN	1183	1246	1612

### 3.4 Adhesion

During scratch test, friction force and coefficient of friction were recorded online along with the indenter movement to confirm the critical loads for cracks, chipping, delamination, coating failure and other such events. Tests performed at different loading rates were observed to give almost similar results and variation in loading rate had little impact on the

scratching behavior. As the scratch progressed small cracks, long wide cracks, pores, chipping, partial and complete delamination of the coating events were observed with increasing load. Fig. 2 shows the scratch patterns for NbN/MS; at 9N load the pattern showed the chipping at few places while at 28N load the coating delaminated nearly completely. Fig. 3 exhibits the scratch patterns for NbN/SS at various loads. Scratch at 3N load showed underneath layer of different colour with no damage; at 8N load, segregation, and pores were visible though coating was still intact; at 13N load, pores density increased a lot and chipping, pores and pile-up appeared; at 30N load coating was found to delaminate partly at many places. This demonstrates the coatings showed much better performance on SS than on MS samples. However when NbN/MS with EN interlayer (10 $\mu\text{m}$  thick) was scratch tested, it performed equally or even better than NbN/SS (Fig.4). Comparing the scratch patterns of NbN/SS (Fig.3) and NbN/EN/MS (Fig.4) at the same loads, NbN/EN/MS revealed less damage with respect to chipping, cracks, pores and delamination.

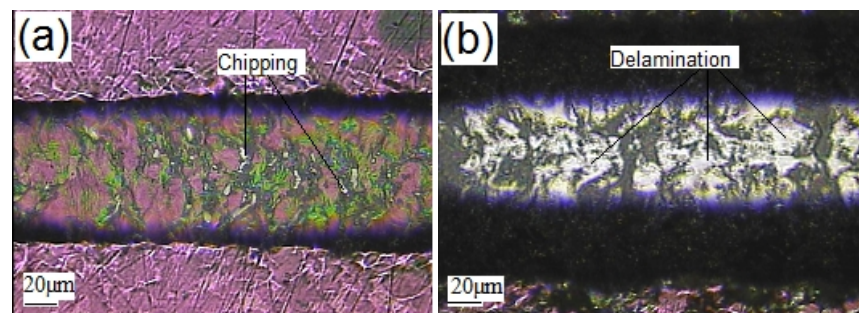


**Fig. 2. Scratch test for NbN coating on MS at (a) 9N load showing chipping and (b) 28N load showing nearly complete delamination**

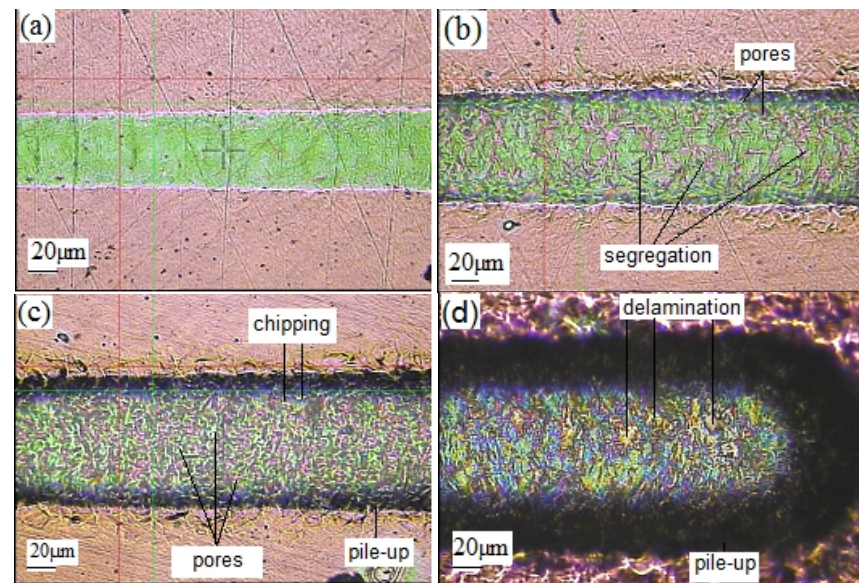


**Fig. 3. Scratch test for NbN coating on SS at (a) 3N load showing underneath layer with no damage; (b) 8N load revealing segregation and pores; (c) 13N load displaying chipping, pores, pile-up; and (d) 30N load showing pile-up and delamination**

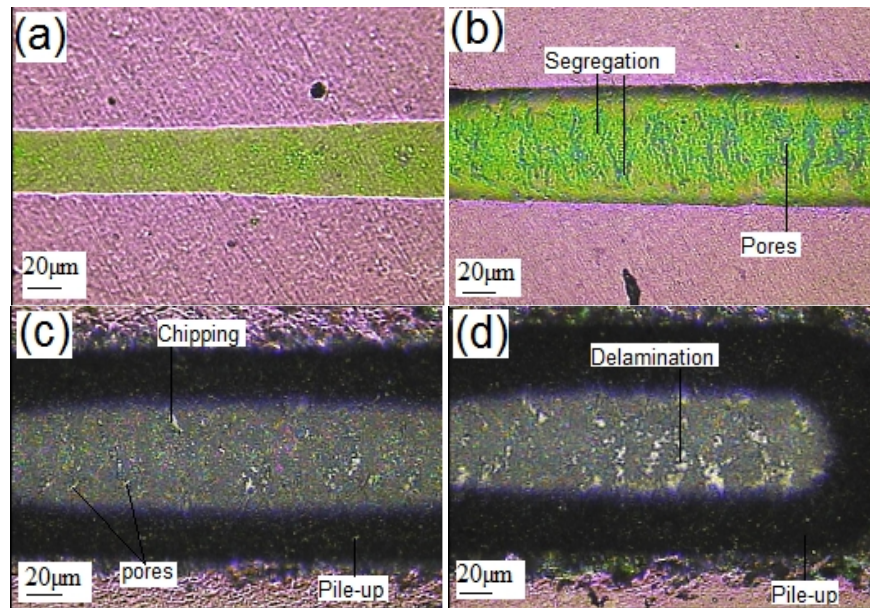


**Fig. 4. Scratch test for NbN/EN/MS at (a) 1N load showing start of the scratch; (b) 12N load revealing segregation and pores; (c) 22N displaying chipping, pores, pile-up; and (d) 32N load showing pile-up and partial delamination**

Two critical loads  $L_{c_1}$  and  $L_{c_2}$  have been defined for the failure of the coatings during scratch tests.  $L_{c_1}$  (the first critical load) corresponds to initial cohesive failure of the coating such as appearance of first cracks or pores within the coating.  $L_{c_2}$  (the second critical load) corresponds to adhesive failure of the coating i.e. first observation of adhesive failure such as chipping, partial delamination, pores or some such event, where substrate beneath coating gets exposed.  $L_{c_1}$  and  $L_{c_2}$  for NbN/MS were observed to be between 6-8N and 9-12N loads respectively. For NbN/SS,  $L_{c_1}$  varied between 8-15N and  $L_{c_2}$  between 12-25N.

NbN/SS thus showed better performance than NbN/MS. However, for NbN/EN/MS the critical loads improved;  $L_{c_1}$  varied between 8-18N and  $L_{c_2}$  between 10-28N, showing either equal or even better performance than NbN/SS. The critical load of the CrN/MS was also found to increase when incorporated with EN interlayer [37].

Coefficient of friction ( $\mu$ ), as observed in the scratch adhesion test, varied with the scratch load. For NbN/SS samples, the value varied within a narrow range of 0.22-0.25 at 30N load irrespective of coatings deposited at different flow ratios of  $N_2$ .  $\mu$  increased as the scratch load was increased. Table 3 lists the  $\mu$  value at different loads for NbN coating on MS, SS EN/MS. NbN/MS samples showed higher coefficient of friction than NbN/SS samples at the same applied scratch load. However, for NbN/MS with EN interlayer the  $\mu$  decreased at all the tested loads, clearly demonstrating the improvement. Some related studies have reported that the  $H/E$  ratio ( $H$ =Hardness of the materials and  $E$ =Modulus of Elasticity) was one of the important factors to influence the wear behavior of coatings [38-40]. Higher  $H/E$  ratio results in a lower  $\mu$  value. In general, EN coating has a higher  $H/E$  ratio as compared to MS. Therefore, when EN interlayer was incorporated with NbN/MS,  $\mu$  decreased. In the study by Wu et al [25], it was found that the presence of a single CrN coating reduced the wear depth significantly as compared to the substrate and thus promotes the wear

resistance of the MS; however after the introduction of the EN interlayer, the fluctuation of the cross-section profile was further flattened out.

**Table 3.  $\mu$  at different loads for NbN coating on MS, SS and EN/MS**

Load(N)	MS	SS	EN/MS
20	0.23	0.20	0.18
30	0.28	0.25	0.22
40	0.35	0.30	0.28
60	0.45	0.40	0.37

Depth of penetration during scratch tests increased with the increase in applied load. At 30N load, on an average, NbN/MS samples had 20-30  $\mu\text{m}$  depth of penetration while NbN/SS samples had 12-25  $\mu\text{m}$  depth of penetration. NbN/MS with EN interlayer reduced the depth of penetration to 10-22  $\mu\text{m}$  at the same loads indicating the good load support provided by the interlayer. Depth of penetration includes elastic as well as plastic deformation during loading.

### 3.5 Corrosion Resistance

Coatings deposited by PVD techniques generally show pin-hole porosity. Therefore, the electrochemical behavior of the PVD coated sample in a corrosive environment shows the combined behavior of the coating and the substrate. The polarization curve of such a specimen may be considered as a combination of two curves - one representing the base material, and the other the coating.

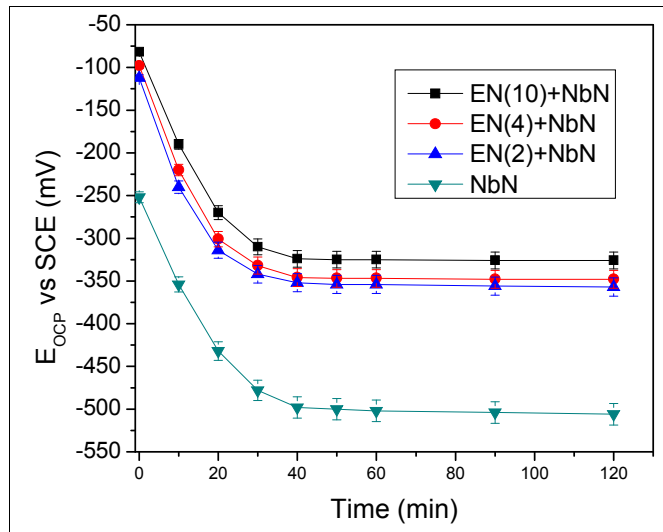
#### 3.5.1 Open Circuit Potential

Fig.5 shows the changes in open circuit potential with immersion time for NbN/MS as such and with EN interlayer in various thicknesses. For NbN/MS without interlayer, potential decreased from an initial value of -252mV to -478mV in 30min and to -498mV in 40 min; after which it remained nearly constant indicating the establishment of equilibrium between the metal and the solution. The equilibrium value was quite similar to MS substrate without coating, thus indicating the presence of pores in the coating, resulting in corrosion taking place beneath NbN coating. For NbN/MS with EN interlayer, the OCP's shifted to -82, -98 and -112mV in the beginning for 10, 4 and 2 $\mu\text{m}$  thick interlayer respectively from -252mV for coating without interlayer. The values decreased to -324, -346 and -352mV for 10, 4 and 2 $\mu\text{m}$  thick EN interlayer after 40min. The values remained constant thereafter. This clearly demonstrated improvement in the corrosion resistance of the coated samples when incorporated with EN interlayer.

#### 3.5.2 Potentiodynamic Tests

$E_{\text{corr}}$  and  $I_{\text{corr}}$  were determined from the polarization curves using the Tafel slopes ( $\beta_a$ ,  $\beta_c$ ) and polarization resistance ( $R_p$ ). A high  $E_{\text{corr}}$  and a low  $I_{\text{corr}}$  values are indicative of good corrosion resistance. Table 4 lists the  $E_{\text{corr}}$  and  $I_{\text{corr}}$  values for MS substrate, NbN/MS, EN/MS, and NbN/MS with EN interlayer in different thicknesses. Plain MS substrate had  $I_{\text{corr}}$  value of 1440 $\mu\text{A}/\text{cm}^2$ . Coating the MS with NbN improved the corrosion resistance by decreasing the  $I_{\text{corr}}$  to 150 $\mu\text{A}/\text{cm}^2$  and increasing the  $E_{\text{corr}}$  (less negative) to -412mV. However, the improvement was constrained due to the presence of pin-hole porosity inherent in the PVD

coatings. Due to the presence of pin-hole defects in the NbN coatings, in fact rapid pitting corrosion of MS substrate takes place at these defects; even leading to partial debonding of the coating during the tests. The potentiodynamic curves for NbN/MS, therefore, mimic the behavior of MS substrate.



**Fig. 5.  $E_{OCP}$  Vs time for NbN/MS and NbN/EN/MS (EN=2, 4 and 10 $\mu$ m thick) in 1N  $H_2SO_4$ . Standard deviations are shown as error bars in the plot**

**Table 4.  $E_{corr}$  and  $I_{corr}$  values for single and duplex coatings**

Coating (thickness $\mu$ m)	$E_{corr}$ (mV)	$I_{corr}$ ( $\mu$ A/cm $^2$ )	Coating (thickness $\mu$ m)	$E_{corr}$ (mV)	$I_{corr}$ ( $\mu$ A/cm $^2$ )
Substrate	-496.4	1440.3	NbN/MS	-412.1	150.2
EN (2)	-339.3	8.6	EN (2) + NbN	-320.3	2.3
EN (4)	-330.4	0.24	EN (4) + NbN	-294.6	0.37
EN (10)	-214.3	0.21	EN (10) + NbN	-220.6	0.35

EN as interlayer improved the corrosion resistance of NbN coated MS substrates remarkably. For 10 $\mu$ m thick EN interlayer  $E_{corr}$  and  $I_{corr}$  values were found to be -220.6mV and 0.35 $\mu$ A/cm $^2$  respectively. Improvement in adherence of the duplex coatings was also demonstrated by the potentiodynamic tests. None of the coatings was found to delaminate for the full potential sweep of -1000mV to +1000mV during the potentiodynamic corrosion tests performed for all the interlayer thicknesses. Potentiodynamic curves for MS substrate; NbN/MS, EN/MS and NbN/MS with EN interlayer are shown in Fig.6. Potentiodynamic curves for the duplex coatings show a remarkable improvement in corrosion improvement for MS substrate. In general, it was observed that the duplex coatings are much superior to untreated substrate and to the NbN coatings alone. The optimum thickness of EN interlayer was observed to be 4  $\mu$ m. Remarkable improvement in the corrosion resistance was also observed by Grips et al [8] for TiN and CrN coatings on MS when incorporated with EN interlayer.

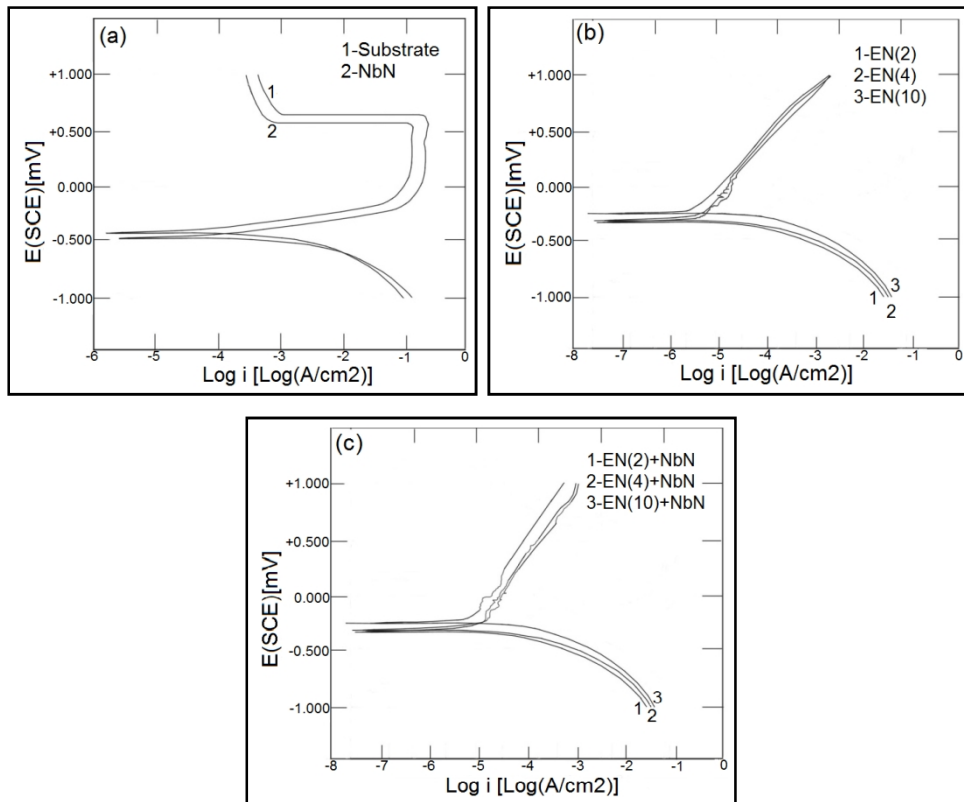


**Fig. 6. Potentiodynamic curves for (a) MS and NbN/MS; (b) EN/MS and (c) NbN/EN/MS**

#### 4. CONCLUSION

NbN coatings were deposited by reactive DC magnetron sputtering. N<sub>2</sub>/Ar flow ratio was varied from 5 to 70% and substrate biasing from zero to -150V. Coatings were characterized for their thickness by weight gain and Calo test technique, hardness by Knoop micro hardness tester, phase analysis by XRD and adhesion by scratch tester. After the optimization of process parameters, NbN coatings were deposited on MS substrate with EN interlayer. EN was deposited by electroless plating in 2, 4 and 10 μm thickness. Effect of interlayer on NbN coating on MS was studied for improvement in adhesion, hardness and corrosion. Corrosion test was performed by potentiodynamic polarization technique in 1N H<sub>2</sub>SO<sub>4</sub> solution at room temperature. XRD showed the presence of hexagonal β Nb<sub>2</sub>N, cubic δ NbN and hexagonal δ' NbN phases with increasing N<sub>2</sub> flow. Surface hardness increased from 1084HK<sub>25</sub> for NbN/MS to 1436, 1564 and 1612 HK<sub>25</sub> when EN was incorporated as interlayer in 2, 4 and 10 μm thickness. In the scratch tests, critical load for cohesive failure (L<sub>c1</sub>) varied between 6-8N, 8-15N and 8-18N and critical load for adhesive failure (L<sub>c2</sub>) varied between 9-12N, 12-25N and 10-28N for NbN/MS, NbN/SS and NbN/EN/MS respectively. Coatings deposited at 20-30% of N<sub>2</sub>/Ar flow ratios and substrate biasing at -50 and -75V, showed better adhesion with higher critical loads for failure. Variation in loading rate during scratch test had little impact on the critical loads. Coefficient of friction (μ) (during scratch adhesion test) was 0.25 at 30N, 0.30 at 40N and 0.40 at 60N load for NbN/SS. For NbN/MS, the μ was 0.28 at 30N, 0.35 at 40N and 0.45 at 60N load. However, For

NbN/EN/MS,  $\mu$  decreased to 0.22, 0.28 and 0.37 at 30, 40 and 60N loads respectively, demonstrating the improvement. For corrosion protection, it was observed that NbN coating alone could not protect the MS substrate effectively. EN as interlayer was effective in protecting the MS substrate. With duplex coating, the corrosion resistance increased enormously.  $I_{corr}$  decreased from  $150.2\mu A/cm^2$  for NbN/MS to 2.3, 0.37 and  $0.35\mu A/cm^2$  with 2, 4 and 10  $\mu m$  thick EN interlayer respectively.

## ACKNOWLEDGEMENTS

Authors wish to express their gratitude to Director, Materials Group for encouraging and providing support and sincerely thank to Mr. A. L. Pappachan for the help provided in depositing EN interlayer.

## COMPETING INTERESTS

Authors have declared that no competing interests exist.

## REFERENCES

1. Lin J, Wu ZL, Zhang XH, Mishra B, Moore JJ, Sproul WD. A comparative study of CrNx coatings Synthesized by dc and pulsed dc magnetron sputtering. *Thin Solid Films*. 2009;517(6):1887-94.
2. Oya T, Kusano E. Effects of radio-frequency plasma on structure and properties in Ti film deposition by dc and pulsed dc magnetron sputtering. *Thin Solid Films*. 2009;517(20):5837-43.
3. Zeng D, Jie W, Zhou H, Yang Y. Effect of sputtering power on the properties of Cd<sub>1-x</sub>Znx Te films deposited by radio frequency magnetron sputtering. *Thin Solid Films*. 2011;519(13):4158-61.
4. Barshilia HC, Deepthi B, Rajam KS. Growth and characterization of aluminum nitride coatings prepared by pulsed-direct current reactive unbalanced magnetron sputtering. *Thin Solid Films*. 2008;516(12):4168-74.
5. Chen J-S, Duh J-G, Wu F-B. Microhardness and corrosion behavior in CrN/electroless Ni/mild steel complex coating. *Surf. Coat. Technol.* 2002;150(2-3):239-245.
6. Singh K, Grover AK, Totalani MK, Suri AK. TiN coatings on nickel and electroless nickel (EN) plated mild steel. *Trans. IMF*. 2000;78(1):23-28.
7. Singh K, Grover AK, Totalani MK, Suri AK. TiN coatings modified by an interlayer of electroplated chromium on mild steel. *Trans. IMF*. 1999;77(5):196-201.
8. Grips VKW, Selvi VE, Barshilia HC, Rajam KS. Effect of electroless nickel interlayer on the electrochemical behavior of single layer CrN, TiN, TiAlN coatings and nanolayered TiAlN/CrN multilayer coatings prepared by reactive dc magnetron sputtering. *Electrochimica Acta*. 2006;51(17):3461-68.
9. Subramanian B, Ashok K, Jayachandran M. Characterization of reactive magnetron sputtered nanocrystalline titanium nitride (TiN) thin films with brush plated Ni interlayer. *J Appl. Electrochem.* 2007;37(9):1069-74.
10. Benkahoul M, Martinez E, Karimi A, Sanjin'es R, L'evy F. Structural and mechanical properties of sputtered cubic and hexagonal NbNx thin films. *Surf. Coat. Technol.* 2004;180/181:178-183.
11. Al'en P, Ritala M, Arstila K, Keinonen J, Leskela M. The growth and diffusion barrier properties of atomic layer deposited NbNx thin films. *Thin Solid Films*. 2005;491(1-2):235-241.

12. Kim SK, Cha BC, Yoo JS. Deposition of NbN thin films by DC magnetron sputtering process. *Surf. Coat. Technol.* 2004;177/178:434-440.
13. Sandu CS, Benkahoul M, Parlinska-Wojtan M, Sanjinés R, Lévy F. Morphological, structural and mechanical properties of NbN thin films deposited by reactive magnetron sputtering. *Surf. Coat. Technol.* 2006;200(22-23):6544-46.
14. Fenker M, Balzer M, Kappl H. Corrosion behaviour of decorative and wear resistant coatings on steel deposited by reactive magnetron sputtering – Tests and improvements. *Thin Solid Films.* 2006;515(1):27-32.
15. Olaya JJ, Rodil SE, Muhl S. Comparative study of niobium nitride coatings deposited by unbalanced and balanced magnetron sputtering. *Thin Solid Films.* 2008;516(23):8319-26.
16. Klingenberg ML, Demaree JD. The effect of transport ratio and ion energy on the mechanical properties of IBAD niobium nitride coatings. *Surf. Coat. Technol.* 2001;146/147:243-249.
17. Hayashi N, Murzin IH, Sakamoto I, Ohkubo M. Single-crystal niobium nitride thin films prepared with radical beam assisted deposition. *Thin Solid Films.* 1995;259(2):146-149.
18. Cappuccio G, Gambardella U, Morone A, Orlando S, Parisi GP. Pulsed laser ablation of NbN/MgO/NbN multilayers. *Appl. Surf. Sci.* 1997;109/110:399-402.
19. Cansever N, Danışman M, Kazmanlı K. The effect of nitrogen pressure on cathodic arc deposited NbN thin films. *Surf. Coat. Technol.* 2008;202(24):5919-23.
20. Bendavid A, Martin PJ, Kinder TJ, Preston EW. The deposition of NbN and NbC thin films by filtered vacuum cathodic arc deposition. *Surf. Coat. Technol.* 2003;163:347-52.
21. Mo JL, Zhu MH. Tribological characterization of chromium nitride coating deposited by filtered cathodic vacuum arc. *App. Surf. Sci.* 2009;255(17):7627-34.
22. Cansever N. Properties of niobium nitride coatings deposited by cathodic arc physical vapor deposition. *Thin Solid Films.* 2007;515(7-8):3670-74.
23. Cunha L, Andritschky M, Pischedow K, Wang Z. Microstructure of CrN coatings produced by PVD techniques. *Thin Solid Films.* 1999;355/356:465-471.
24. Singh K, Krishnamurthy N, Suri AK. Adhesion and wear studies of magnetron sputtered NbN films. *Tribology International.* 2012;50:16–25.
25. Wu F-B, Li J-J, Duh J-G. Evaluation of the mechanical properties and tribological behavior of the CrN coating deposited on mild steel modified with electroless Ni interlayer. *Thin Solid Films.* 2000;377/378:354–359.
26. Wokulski Z. Mechanical Properties of TiN Whiskers. *Phys. Status Solidi.* 1990;120(1):175-182.
27. Chou WJ, Yu GP, Huang JH. Deposition of TiN thin films on Si(100) by HCD ion plating. *Surf. Coat. Technol.* 2001;140(3):206-214.
28. Nadia Saoula N, Henda K, Kesri R. influence of nitrogen content on the structural and mechanical properties of TiN Thin Films. *J. Plasma Fusion Res. Series.* 2009;8:1403-07.
29. Meng LJ, Santos MPdos. Characterization of titanium nitride films prepared by d.c. reactive magnetron sputtering at different nitrogen pressures. *Surf. Coat. Technol.* 1997;90(1-2):64-70.
30. Čekada M, Panjan P, Maček M, PetrŠmíd. Comparison of structural and chemical properties of Cr-based hard coatings. *Surf. Coat. Technol.* 2002;151/152:31-35.
31. Wuhrer R, Yeung WY. An empirical analysis of nitrogen pressure effect on grain size development of nanostructured ternary nitride coatings. *Materials Forum,* 2005;29:103-110.

32. Veprek S, Veprek-Heijman MGJ, Karvankova P, Prochazka J. Different approaches to superhard coatings and nanocomposites. *Thin Solid Films.* 2005;476(1):1-29.
33. Bunshah RF. *Handbook of Deposition Technologies for Films and Coatings.* 2nd ed. Park Ridge: Noyes Publications; 1994.
34. Lee JW, Tien SK, Kuo YC. The effects of pulse frequency and substrate bias to the mechanical properties of CrN coatings deposited by pulsed DC magnetron sputtering. *Thin Solid Films.* 2006;494(1-2):161-167.
35. Herr W, Broszeit E. The influence of a heat treatment on the microstructure and mechanical properties of sputtered coatings. *Surf. Coat. Technol.* 1997;97(1-3):335-340.
36. Ljungcrantz H, Hultman L, Sundgren J-E. Ion induced stress generation in arc-evaporated TiN films. *J. Appl. Phys.* 1995;78(2):832-840.
37. Wu F-b, Duh J-g. Scratch behavior and in situ acoustic emission analysis of PVD chromium nitride coatings on mild steel with electroless nickel interlayers. *Surf. Coat. Technol.* 2003;162(1):106-112.
38. Leyland A, Matthews A. On the significance of the H/E ratio in wear control: a nanocomposite coating approach to optimised tribological behaviour. *Wear.* 2000;246(1-2):1-11.
39. Hsu CH, Lee CC, Ho WY. Filter effects on the wear and corrosion behaviors of arc deposited (Ti,Al)N coatings for application on cold-work tool steel. *Thin Solid Films.* 2008;516:4826-32.
40. Lin C-K, Hsu C-H, Kung S-C. Effect of electroless nickel interlayer on wear behavior of CrN/ZrN multilayer films on Cu-alloyed ductile iron. *Applied Surface Science.* 2013;284:59-65.

© 2014 Singh et al.; This is an Open Access article distributed under the terms of the Creative Commons Attribution License (<http://creativecommons.org/licenses/by/3.0>), which permits unrestricted use, distribution, and reproduction in any medium, provided the original work is properly cited.

*Peer-review history:*

*The peer review history for this paper can be accessed here:*

<http://www.sciedomain.org/review-history.php?iid=471&id=22&aid=4086>